

A Computational Approach to Investigate Electromagnetic Shielding Effectiveness of Steel Fiber-Reinforced Mortar

S.H. Kwon¹ and H.K. Lee²

Abstract: The electromagnetic shielding effectiveness of steel fiber-reinforced mortar was numerically examined in this study. A series of numerical analysis on twenty-seven types of specimens of different diameters, lengths, and volume fractions of fibers were conducted using the FE program HFSS to investigate the effect of the dimensions of steel fibers and the amount of fibers added to the mortar on the shielding effectiveness. S-parameters of some specimens were experimentally measured by the free space method and the experimentally measured S-parameters were compared with those computed in order to verify the present numerical analysis method. It was found that smaller diameters and larger volume fractions provided better shielding effectiveness. Fiber length did not strongly influence the shielding effectiveness. The number of fibers was found to strongly influence the shielding of electromagnetic waves, and the optimal number of fibers in the mortar was found.

Keywords: Fiber Reinforcement, Finite Element Analysis, Electrical Properties, Electromagnetic Shielding.

1 Introduction

Residential and work environments are surrounded by a high volume of electromagnetic waves originating from sources such as mobile phones, wireless internet networks, appliances, and radio communication. These electromagnetic waves may interfere with one another, potentially leading to the malfunction of electronic devices and noise in the communication [Wen and Chung (2004)].

The present study is a part of a project to develop technologies to enhance electromagnetic compatibility inside buildings. The project provides the means of shield-

¹ Department of Civil and Environmental Engineering, Myongji University, San 38-2, Namdong, Cheoin-gu, Yongin, Gyeonggi-do, 449-728, South Korea

² Department of Civil and Environmental Engineering, Korea Advanced Institute of Science and Technology, Guseongdong 373-1, Yuseong-gu, Daejeon, 305-701, South Korea

ing the electromagnetic waves that penetrate a building from the outside. The broadband frequency protected by the shielding is then exploited to allow safe and clean (person to person or device to device) wireless communication inside the building. One effective way to shield an entire building from outside electromagnetic waves is to construct the building with shielding materials.

One branch of the project to which this study belongs is focused on developing a cement-based material that satisfies requirements for both mechanical performance and electromagnetic shielding. Addition of a conductive and stiff material to cement based mix will be a way to achieve both requirements. Steel fiber and carbon nanotube were originally considered as a possible material to be added to the mix. Steel fiber has been widely used in real construction sites and is economically attractive compared to carbon nanotube. Although many researches on carbon nanotube have been recently performed to enhance mechanical properties and electromagnetic shielding effectiveness of base materials [Ghanbari and Naghdabadi (2009); Charkrabarty and Cargin (2008); Xie, Han and Long (2007)], carbon nanotube is still far from universal usage in construction practice. In this study, the electromagnetic shielding effectiveness of steel fiber-reinforced mortar was numerically examined. It is well known that the addition of steel fibers to cement-based materials is an effective mean of reducing crack width and enhancing ductility. Recently, a research group at the University at Buffalo revealed the excellent shielding ability of steel fibers, from which a shielding effectiveness of 70dB at 1.5GHz has been attained using a cement paste that contains 0.72 vol.% stainless steel fibers of 8 μ m diameter and 6mm length [Wen and Chung (2004)]. In addition to that finding, the shielding effectiveness of cement-based composites has been extensively investigated [Fu and Chung (1997); Chiou, Zheng and Chung (1989); Fu and Chung (1998)] by the same research group. For the sake of electromagnetic shielding, the existing studies [Wen and Chung (2004); Fu and Chung (1997); Chiou, Zheng and Chung (1989); Fu and Chung (1998)] imply that it is desirable to increase the number of fibers by using thin fibers while maintaining the same volume fraction of steel fibers within the mortar. However, producing a large bulk of cement-based material reinforced with thin fibers having a diameter of less than 50 μ m would present serious challenges in practice.

For mechanical considerations, 0.15 to 0.50 mm diameter fibers are widely used in practice [Shah and Naaman (1976); Felekoglu, Turkel and Altuntas (2007); Rahimi and Kesler (1979)]. The employment of fibers incorporated for mechanical purposes as electromagnetic shielding presents an optimal way to simultaneously achieve both the required mechanical performance and electromagnetic shielding ability. Concrete could be considered as a base material to which fibers are added, but large aggregates may disturb the uniform distribution of the fibers, a factor that is impor-

tant for electromagnetic shielding. For economic reasons, the use of cement paste as a base material is not practical. Therefore, mortar was selected as a base material in this study. In concrete, fibers of 20mm to 50mm length are usually used. However, in the case of mortar, the fracture process zone is much smaller than that of concrete because there is no bridging effect from aggregates, and shorter fibers can be used to prevent cracking [Bazant and Planas (1998);Gonzalez, Maimi, Turon, Camanho and Renart (2009); Ferretti and Leo(2008)]. In previous studies, 6mm to 13mm long fibers have been used in steel fiber-reinforced mortar [Shah and Naaman (1976);Felekoglu, Turkel and Altuntas (2007);Rahimi and Kesler (1979)]. For mechanical purposes, fibers are usually added in quantities as high as 1 to 3% of the total volume of the base material. In this study, the effect of steel fiber-reinforced mortar on electromagnetic shielding is numerically investigated according to different volume fractions (1%-3%), different diameters (0.16mm-0.5mm), and different lengths of fibers (6mm-12mm). Further, S parameters of some specimens were experimentally measured by the free space method and the experimentally measured S parameters were compared with those computed in order to verify the present numerical analysis method.

There are two types of tests for electromagnetic shielding effectiveness: the coaxial cable method and the free space method [Wen and Chung (2004);Ghodgaonkar, Varadan and Varadan (1989);Kim and Lee (2009)]. The test results will potentially be very sensitive to the inevitable errors induced in the process of manufacturing the specimens, particularly because they are formed of a cement-based material; such errors could be reflected as surface roughness, voids on the surface, non-uniform distribution of fibers, or as the influence of external humidity conditions, temperature, and so on. Therefore, it is preferred to assess electromagnetic shielding effectiveness according to the parametric analysis noted above, before planning and performing the tests. Furthermore, the randomly distributed fibers inside the base material are fully modeled in the electromagnetic simulation performed in this study; such a numerical approach based on full modeling of the composite has been rarely attempted.

2 S-parameters and electromagnetic properties

2.1 S-parameters

The electromagnetic shielding effectiveness of materials can be quantitatively expressed by S-parameters [Wen and Chung (2004)]. Fig. 1 shows a schematic of a waveguide in the middle of which a material is inserted. From one of both ends, an electromagnetic wave is radiated. At the surface of the material, a part of the incident wave is reflected, and the other part penetrates the material. A part of the

penetrating wave is absorbed inside the material, and the other part is transmitted through the material. The process of reflection, absorption, and transmission is called scattering of the wave, and the S-parameter represents that scattering.

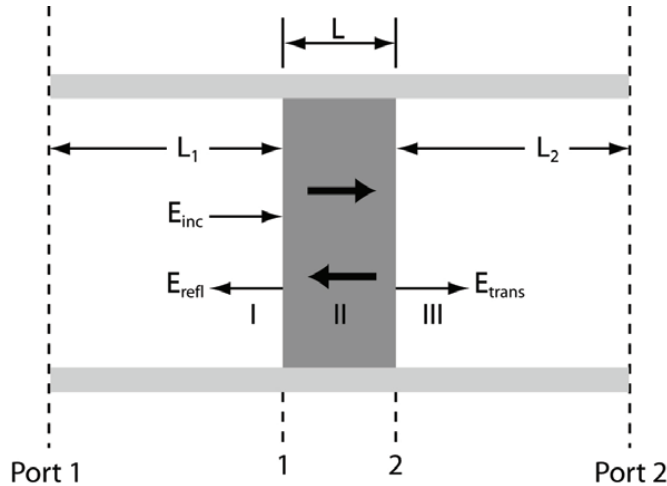


Figure 1: Specimen in the middle of waveguide and electric field distributions in regions I, II, and III [Bazant and Planas (1998)]

In the figure, the incident wave from the left end (port 1) progresses towards the right end (port 2). When the material is homogenous, the scattering parameters of a 2-port device are expressed by the following [Baker-Jarvis, Vanzura and Kissick (1990)].

$$S_{11} = R_1^2 \left[\frac{\Gamma(1 - T^2)}{1 - \Gamma^2 T^2} \right] \quad (1)$$

$$S_{22} = R_2^2 \left[\frac{\Gamma(1 - T^2)}{1 - \Gamma^2 T^2} \right] \quad (2)$$

$$S_{21} = R_1 R_2 \left[\frac{T(1 - \Gamma^2)}{1 - \Gamma^2 T^2} \right] \quad (3)$$

$$S_{12} = R_2 R_1 \left[\frac{T(1 - \Gamma^2)}{1 - \Gamma^2 T^2} \right] \quad (4)$$

where

$$R_1 = \exp(-\gamma_0 L_1) \quad (5)$$

$$R_2 = \exp(-\gamma_0 L_2) \quad (6)$$

in which L_1 is the distance from port 1 to the left end of the specimen, while L_2 is the distance from port 2 to the right end of the specimen. If the material is homogenous, the parameter S_{21} is identical to S_{12} since the scattering matrix should be symmetric [Baker-Jarvis, Vanzura and Kissick(1990)]. In addition, the reflection coefficient Γ and the transmission coefficient T are given as follows [Baker-Jarvis, Vanzura and Kissick (1990)].

$$\Gamma = \frac{\frac{\gamma_0}{\mu_0} - \frac{\gamma}{\mu}}{\frac{\gamma_0}{\mu_0} + \frac{\gamma}{\mu}} \quad (7)$$

$$T = \exp(-\gamma L) \quad (8)$$

where L is the material length, and γ_0 and γ are expressed by the following equations [Baker-Jarvis, Vanzura and Kissick (1990)].

$$\gamma = j \sqrt{\frac{\omega^2 \mu_R^* \epsilon_R^*}{c_{vac}^2} - \left(\frac{2\pi}{\lambda_c}\right)^2} \quad (9)$$

$$\gamma_0 = j \sqrt{\left(\frac{\omega}{c_{vac}}\right)^2 - \left(\frac{2\pi}{\lambda_c}\right)^2} \quad (10)$$

In Eqs. (9) and (10), $j = \sqrt{-1}$, c_{vac} is the speed of the wave under a vacuum, ω is the angular frequency, λ_c is the cutoff wavelength of the waveguide, ϵ_0 and μ_0 are the permittivity and permeability of the vacuum, respectively, and γ_0 and γ are the propagation constants in the vacuum and the material, respectively [Baker-Jarvis, Vanzura and Kissick (1990)]. Further, ϵ_R^* and μ_R^* are the complex permittivity and permeability relative to those under the vacuum as described in the following equations [Baker-Jarvis, Vanzura and Kissick (1990)].

$$\epsilon = [\epsilon_R' - j\epsilon_R'']\epsilon_0 = \epsilon_R^* \epsilon_0 \quad (11)$$

$$\mu = [\mu_R' - j\mu_R'']\mu_0 = \mu_R^* \mu_0 \quad (12)$$

When the lengths L_1 and L_2 are identical, the parameter S_{11} is equal to S_{22} . The parameter S_{ij} is the ratio of the voltage at port i to the voltage at port j . It is also a complex number. Generally, the parameter is represented in dB scale. The complex number of S_{ij} is converted to dB scale as follows [Baker-Jarvis, Vanzura and Kissick (1990); Pozar (2005)].

$$S_{ij} = \alpha + \beta j \quad (13)$$

$$S_{ij}(\text{db}) = 20 \times \log(\sqrt{\alpha^2 + \beta^2}) = 20 \times \log\left(\frac{V_i^-}{V_j^+}\right) \quad (14)$$

In Eq. (14), V_j^+ is the voltage at port j radiating the incident wave, and V_i^- is the voltage at port i receiving the incident wave [Baker-Jarvis, Vanzura and Kissick (1990)]. When S_{11} is equal to zero in dB scale, it means that the incident wave from port 1 is completely reflected from the surface of the material. When the value of S_{21} is zero in dB scale, it means that the incident wave from port 1 is completely transmitted to port 2.

2.2 Electromagnetic properties obtained from the S-parameters

The electromagnetic properties ϵ_R^* and μ_R^* given in Eqs. (11) and (12) can be determined from the S-parameters [Baker-Jarvis, Vanzura and Kissick (1990)]. If the scattering parameters, S_{11} , S_{22} , S_{21} , and S_{12} , are measured on a waveguide, the electromagnetic properties, ϵ_R^* and μ_R^* , can be determined through an inverse analysis. For non-magnetic materials, the parameters μ_R' and μ_R'' in Eq. (12) are 1.0 and 0.0. In the present study, the nonlinear least square optimization proposed in the Marquardt-Levenburg method [Brown (1970)] is utilized to determine the dielectric parameters, ϵ_R' and ϵ_R'' , optimally fitting the S-parameters obtained from the (numerical) parametric analysis.

3 Numerical analysis

3.1 General

In this study, waveguide tests on steel fiber-reinforced mortar with different fiber volume fractions, lengths, and diameters (as illustrated in Fig. 1) are numerically simulated. There are several numerical methods such as finite element, finite difference, finite volume, boundary element methods [Oh, Katsube and Brust (2007); Timmel, Kaliske, Kolling and Mueller (2007); Mai-Duy, Khennane and Tran-Cong (2007)]. In this study, finite element method was exploited in the simulation. Tab. 1 shows the analysis parameters, which were determined by considering the dimensions of fibers being used in practice for mechanical purposes. Fig. 2 shows real steel fibers of $0.16\text{mm} \times 6.0\text{mm}$.

The analysis was performed on a total of twenty-seven mortars. The commercial finite element (FE) program HFSS Ver. 11 [HFSS (2008)] was used. The program utilizes a three-dimensional full-wave FE method to compute the electrical behavior of high-frequency and high-speed components [HFSS (2008)]. Using the program, the mortar was modelled with tetrahedral elements and the convergence was checked from the difference between the S-parameters at the previous and cur-

rent steps as the number of elements was increased. When the difference was found to be less than a predefined tolerance, the analysis was performed with the last mesh refinement, increasing by 0.2 GHz increments from 8.1 GHz to 12.5 GHz. From the results of the analysis, S-parameters were obtained for every analysis parameter.

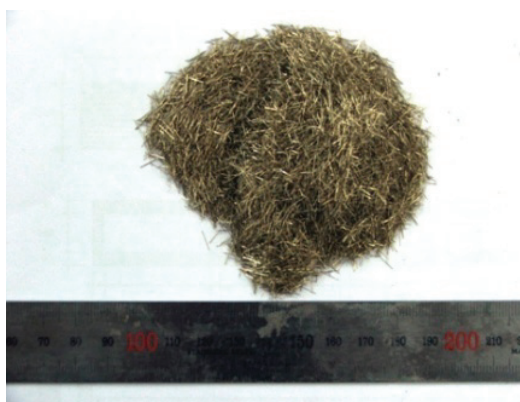


Figure 2: Steel fibers (0.16mm diameter, 6.0mm length)

Table 1: Analysis parameters

Diameter(mm)	Length(mm)	Volume Fraction(%)
0.16	6	1, 2, 3
	9	1, 2, 3
	12	1, 2, 3
0.30	6	1, 2, 3
	9	1, 2, 3
	12	1, 2, 3
0.50	6	1, 2, 3
	9	1, 2, 3
	12	1, 2, 3

In reality, the permittivity of a mortar depends on many factors such as internal humidity, pore or void systems, temperature, and degree of hydration. However, this study is focused on the effect of fibers, and the permittivity of the mortar was assumed to be constant when referred to the previous researches [Wittmann (1975);Halabe, Sotoodehnia, Maser and Kausel(1993)]. The real and imaginary

parts of the assumed relative permittivity for plain mortar were 10.0 and 2.0. The fibers inserted into the mortar mix are generally made of stainless steel to prevent corrosion. The real part of the relative permittivity of stainless steel is 1.0, and its bulk conductivity is 1,100,000 Siemens/m.

3.2 Distribution of steel fibers in mortar matrix

Steel fibers are randomly distributed throughout a mortar in the process of mixing [Li, Zhao and Liu(2008)]. This random distribution must be considered in the modelling of a fiber-reinforced mortar. Fig. 3 shows the procedures for modelling the randomly distributed steel fibers and the specimen inserted in the waveguide. When the dimensions of the specimen simulated in the analysis are $l_1 \times l_2 \times t$ ($l_1 \geq l_2$), and the diameter and length of the fibers are d and l_f , fibers are firstly modelled to be distributed in a cube of $l \times l \times l$, where $l = l_1 + l_f$. If the volume fraction of steel fibers to the total volume of the cube is a_f , and the volume of one steel fiber is v_f , the number of steel fibers distributed in the cube, N , is expressed as the following.

$$N = \frac{V_f}{v_f} = \frac{a_f \times l \times l \times l}{\pi d^2 l_f / 4} \quad (15)$$

The total volume of the cube is divided into N unit cubes, as shown in Fig. 3(a). Both the volume of the unit cube V_{unit} and the length of one edge of the unit cube l_{unit} are given by the following equations.

$$V_{unit} = \frac{V_t}{N} = \frac{l \times l \times l}{N} \quad (16)$$

$$l_{unit} = (V_{unit})^{\frac{1}{3}} \quad (17)$$

The center of each fiber was located at the center of the unit cube, as shown in Fig. 3(b). This is not realistic. However, this configuration was implemented in order to obtain an ideal distribution of fibers and to avoid a biased distribution that would likely arise from a purely random distribution. The direction of the centered fibers was randomly determined in three dimensions. The fiber distribution in the total volume (Fig. 3) had a length, diameter and volume fraction of 6.0mm, 0.16mm and 1%, respectively. Next, the specimen of the rectangular parallelepiped was located in the center of the cube, as shown in Fig. 3(d), and all regions beside it were eliminated, as shown in Fig. 3(e). When fibers intersected, they were assumed to be connected. Finally, the specimen was inserted into the center of the waveguide. The dimensions of the specimen, $l_1 \times l_2 \times t$, were $l_1=19\text{mm}$, $l_2=18\text{mm}$, and $t=5\text{mm}$, respectively. One side of the specimen was intentionally made slightly

different from the other to make the incident wave propagate in the same direction inside the waveguide and to prevent unnecessary error caused in determining the direction of the wave. Fig. 4 shows the notation method for the specimens according to the combination of analysis parameters, where D denotes the diameter in 0.1 millimeter, L the length in millimeter, and % the volume fraction of fibers. The numbers of fibers and (finite) elements in each specimen are listed in Table. 2.

4 Verification of numerical analysis method

Prior to the parametric analysis, S-parameters of a type of the specimens, D16-L6-3%, were measured through the free space test method, as shown in Fig. 5. The test specimen had dimensions of $150 \times 150 \times 5$ mm. Mortar reinforced with the same steel fibers, as shown in Fig. 2, was cast into a mold of the same size. The specimen was demolded a day after casting, and cured for two weeks under 60% relative humidity at 20°. Three companion specimens were prepared, and the test was performed 15 days after casting following Bois et al. [Bois, Benally, Nowak and Zoughi (1998)]. Bois et al. [Bois, Benally, Nowak and Zoughi (1998)] carried out experiments on electromagnetic characterization of cement-based material according to cure-state. It was observed from the experimental results of Bois et al. [Bois, Benally, Nowak and Zoughi (1998)] that the electromagnetic properties become constant after 15 days of curing.

The specimens were installed in the apparatus of the free space measurement system having horn antenna with lenses (8~12GHz frequency range capacity) as shown in Fig. 5. Compared with the conventional free space method, the free space method having horn antenna with lenses has some advantages: 1) concentration of the electromagnetic waves by lenses, 2) requirement of the smaller specimens, 3) more accurate results in comparison with the conventional free space method [Seo, Chin and Lee(2004)].

In order to verify the present numerical analysis method, a comparison between the experimentally measured S-parameters and the S-parameters computed from the present numerical analysis was made, and the results are shown in Fig. 6. For the parameter S21, the calculated values are very close to the measured values at the beginning, at roughly 8.1GHz. However the difference increases with a rise of frequency and decreases after 10GHz for D16-L9-3% and D16-L12-3%. In contrast, the difference of D16-L6-3% continues to rise even after 10GHz. For the parameter S11, the difference monotonically increases with an increase of frequency. In this case, however, the difference is small, unlike in the case of the parameter S21. Considering that errors inevitably occur in experiments and that there is uncertainty regarding the permittivity of the mortar material, the calculated S-parameters can be considered to be close to the measured values. Therefore, it is reasonable to

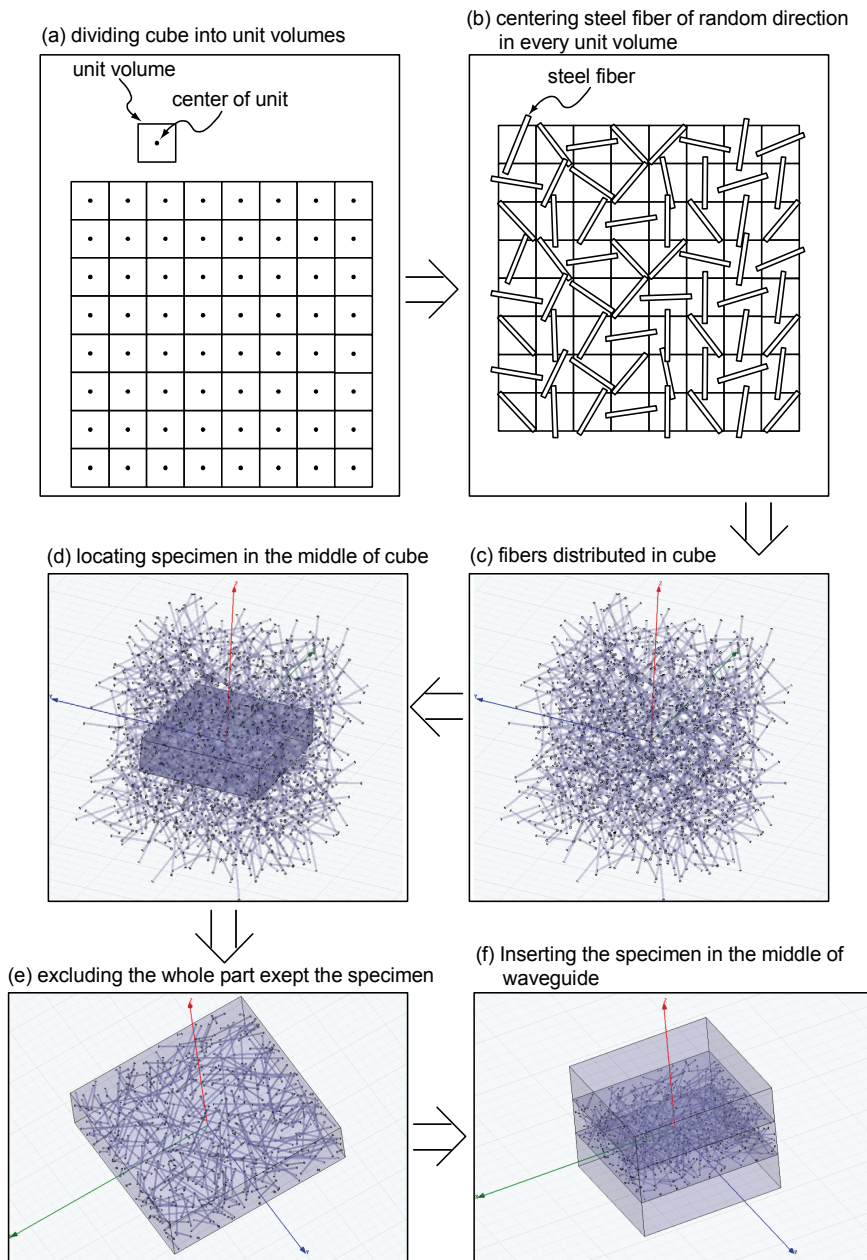


Figure 3: Procedure of modeling randomly distributed steel fibers and the specimen inserted in the waveguide

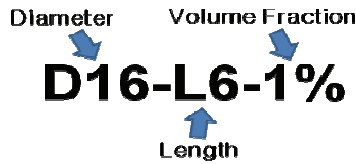


Figure 4: Specimen notation method according to combination of analysis parameters

quantitatively determine the electromagnetic shielding effectiveness of steel fiber reinforced mortar from the FE analysis technique used in this study.

5 Results and discussion

5.1 *S*-parameters

Figure 7 shows the simulated electromagnetic field distribution at 12.5GHz in a vacuum, for plain mortar, and for mortar. The wave is not reflected but is completely transmitted in the waveguide when no material is inserted into the waveguide, as shown in Fig. 7(a). In the case where plain mortar is in the middle of the waveguide as shown in Fig. 7(b), the wave is not transmitted as much as in the case of Fig. 7(a). In the case of mortar (D16-L6-3%), the incident wave from the upper port is almost completely reflected from and absorbed into the material, and it is much less transmitted than when using plain mortar, due to the steel fibers.

The *S*-parameters expressed in dB scale for every specimen are plotted over the frequency axis in Fig. 8. From this graph it is possible to quantitatively determine the magnitude of the effect of the steel fibers on the electromagnetic shielding. First, for the *S*₂₁ parameter, *S*₂₁ increases as its diameter increases, eventually approaching that of plain mortar. This means that the proportion of the wave that is transmitted decreases with the increase of diameter.

As for the *S*₁₁ parameter, *S*₁₁ of plain mortar decreases until 10 GHz and increases thereafter. *S*₁₁ when steel fibers of 0.50mm diameter are used is similar to *S*₁₁ for plain mortar. In contrast to those cases, *S*₁₁ straightens and rises as the diameter of the steel fibers decreases from 0.30 to 0.16mm.

In order to specifically analyze the variation of *S*-parameters according to the volume fraction, length, and diameter of fibers more thoroughly, the *S*-parameters were averaged over frequencies of 8.1GHz to 12.5GHz, and the averaged values are plotted in Fig. 9. In Fig. 9(a), *S*₁₁ slightly increases with an increase of volume fraction, while *S*₂₁ decreases. This indicates that the incident wave from port 1 is reflected more than it is transmitted with an increase of volume fraction. The

Table 2: The number of fibers and elements in the specimens

Specimen	The number of fibers	The number of elements
D16-L6-1%	273	236,275
D16-L6-2%	539	577,252
D16-L6-3%	829	1,169,383
D16-L9-1%	226	278,278
D16-L9-2%	442	502,462
D16-L9-3%	680	1,179,114
D16-L12-1%	223	288,108
D16-L12-2%	420	410,554
D16-L12-3%	614	741,347
D30-L6-1%	88	40,923
D30-L6-2%	158	89,547
D30-L6-3%	209	159,727
D30-L9-1%	67	41,120
D30-L9-2%	118	92,328
D30-L9-3%	199	190,829
D30-L12-1%	62	48,402
D30-L12-2%	109	99,599
D30-L12-3%	176	185,085
D50-L6-1%	21	13,536
D50-L6-2%	56	25,592
D50-L6-3%	91	53,255
D50-L9-1%	22	12,032
D50-L9-2%	49	23,352
D50-L9-3%	70	39,761
D50-L12-1%	17	11,284
D50-L12-2%	42	23,937
D50-L12-3%	62	135,121

impact of diameter is depicted in Fig. 9(b), in which S11 slightly decreases while S21 steeply increases. The variation of S21 for fiber diameters ranging from 0.16 to 0.30mm is much larger than that of S21 for fiber diameters ranging from 0.30 to 0.50 mm. This indicates that the wave is more transmitted when fiber's diameter is increased. In contrast with the volume fraction and diameter, the effect of the fiber's length is not important. This is shown in Fig. 9(c) where S11 and S21 are flatter and have no increasing or decreasing trend according to changes in length. Shield-

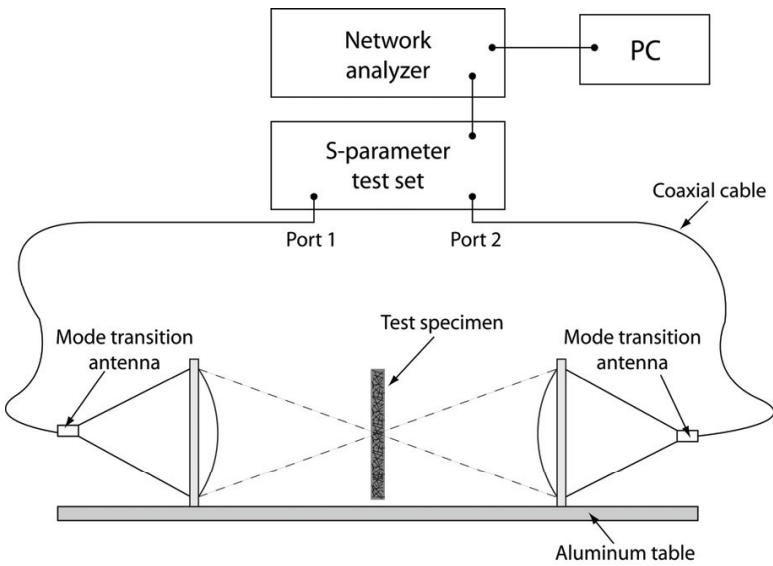


Figure 5: Schematic configuration of the free space test measurement system [Felekoglu, Turkel and Altuntas (2007);Rahimi and Kesler (1979);Brown(1970)]

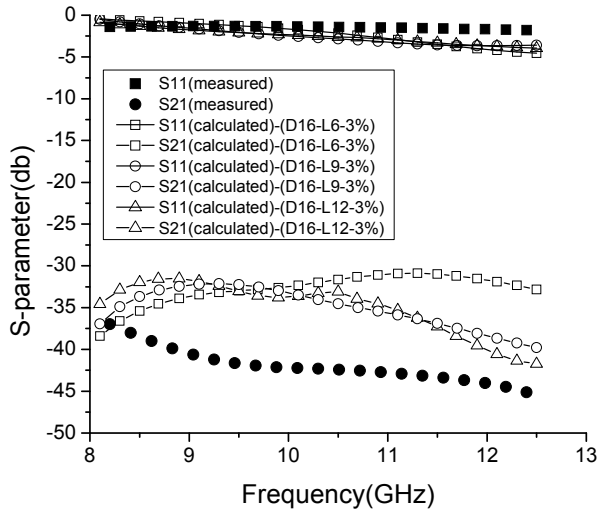
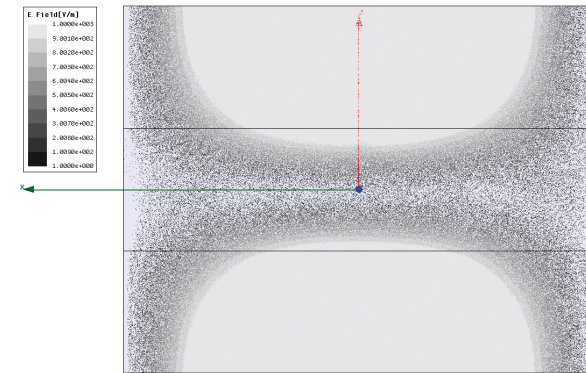
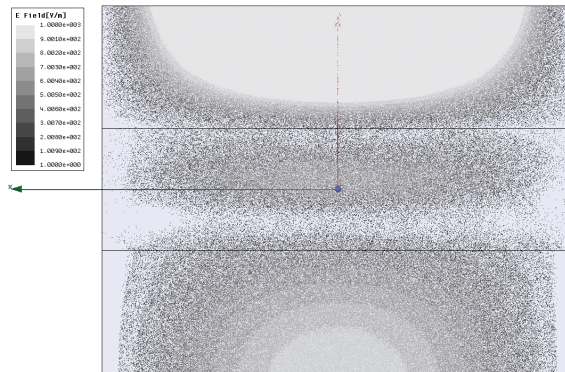


Figure 6: Comparison between measured and calculated S-parameters

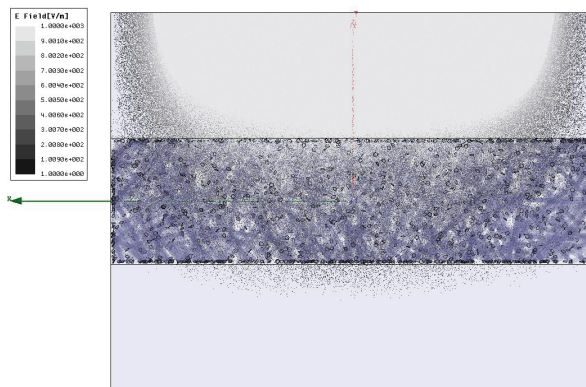
ing effectiveness is directly related to the S21 parameter, because it represents the amount of transmitted waves. Therefore, the diameter and volume fraction of fibers



(a) Vacuum



(b) Plain mortar



(c) Steel fiber-reinforced mortar (D16-L6-3%)

Figure 7: Electric field distribution at 0 phase angle for vacuum, plain mortar, and steel fiber-reinforced mortar

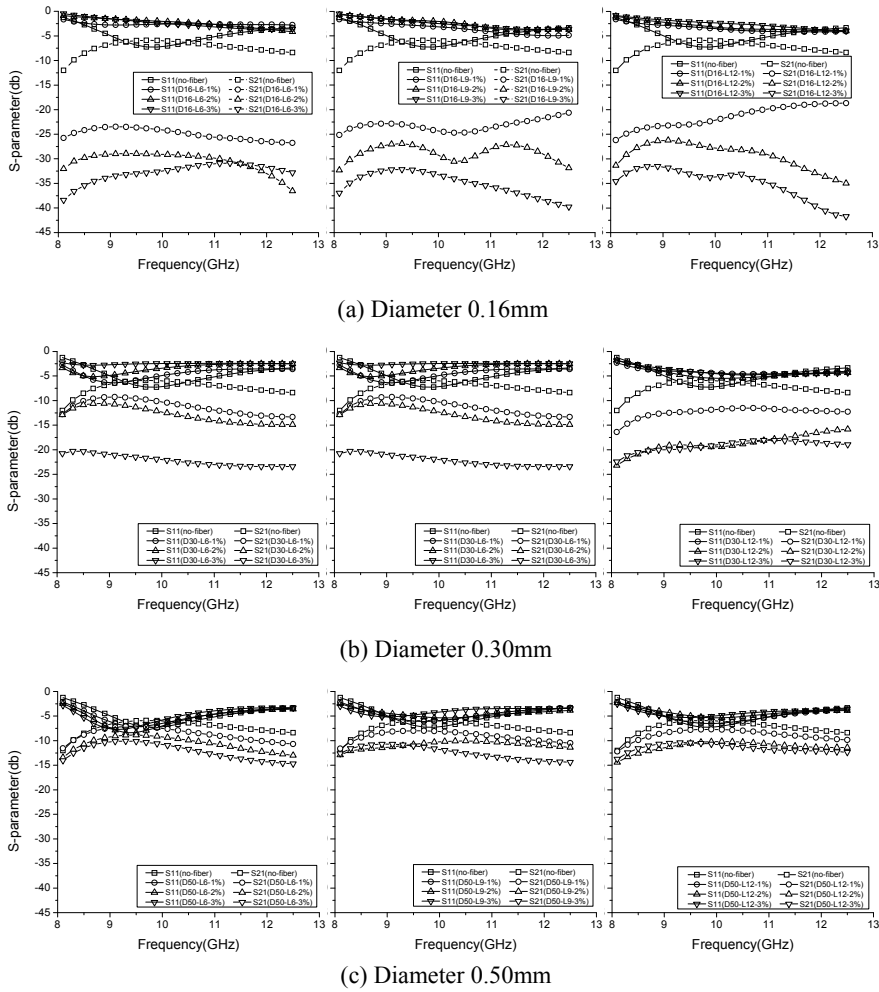


Figure 8: S-parameters obtained from analysis

are the main factors influencing shielding effectiveness. Shielding effectiveness is enhanced by the increase of fiber volume fraction and the decrease of fiber diameter. Maximum shielding effectiveness was achieved in the case where fiber diameter was 0.16mm and the fiber volume fraction was 3%. The average value of S21 for different fiber lengths is -33 dB, indicating that the electric field intensity of the incident wave is reduced as much as 98%.

5.2 Permittivity of steel fiber-reinforced mortar

Multiple studies on methods to determine complex permittivity from S-parameters have been performed [Kim and Lee (2009); Baker-Jarvis, Vanzura and Kissick (1990); Seo, Chin and Lee (2004)]. Generally, for a non-magnetic material, S11 is measured, and the real and imaginary parts of the relative permittivity complex value of S11 are determined [Kim and Lee (2009); Seo, Chin and Lee (2004)]. However, it was found that the permittivity that optimally fits the S11 value obtained from the present analysis yields an erroneous S21 value; the S21 value calculated based on the permittivity determined only from S11 is quite different from the S21 value of the analysis results. Therefore, the permittivity that best fits S11 and S21 was determined in the present study by using the Marquart-Levenburg method [Brown (1970)]. The estimated permittivity thus found for each specimen is plotted over frequency in Fig. 10. Since the permittivity was determined under the assumption that the mortar is a homogenous material, it can be considered as an averaged property of the mortar, given that permittivity highly depends on the interior positioning and direction of fibers within the material when looking at the material on a microscopic level.

Similar to the averaged S-parameters shown in Fig. 9, the real and imaginary parts of the permittivity are averaged over frequencies ranging from 8.1GHz to 12.5GHz, and the averaged values of permittivity are shown in Figs. 11 and 12. The real part of the permittivity for the plain mortar is 10.0. For all the specimens, (except the cases where the fiber diameter is 0.16mm and the fiber volume fractions are 2% and 3%) the real parts are larger than or similar to that of the plain mortar, as shown in Fig. 11(b). As shown in Fig. 11(a), the real part of the permittivity appeared to decrease with an increase of the volume fraction for the fiber diameter 0.16mm, while it gently increased or remained constant for the diameters of 0.30mm and 0.50mm. The values are nearly constant for different fiber lengths, except for the cases D16-L6-1%, D30-L6-2%, and D30-L6-3%, as shown in Fig. 11(c). A clear trend for the real part of permittivity could not be found. However, the imaginary part shows a salient tendency according to the analysis parameters in Fig. 12. It increased with an increase of the volume fraction. Then, it remained nearly constant for the three different lengths of fibers, and decreased as diameter increased.

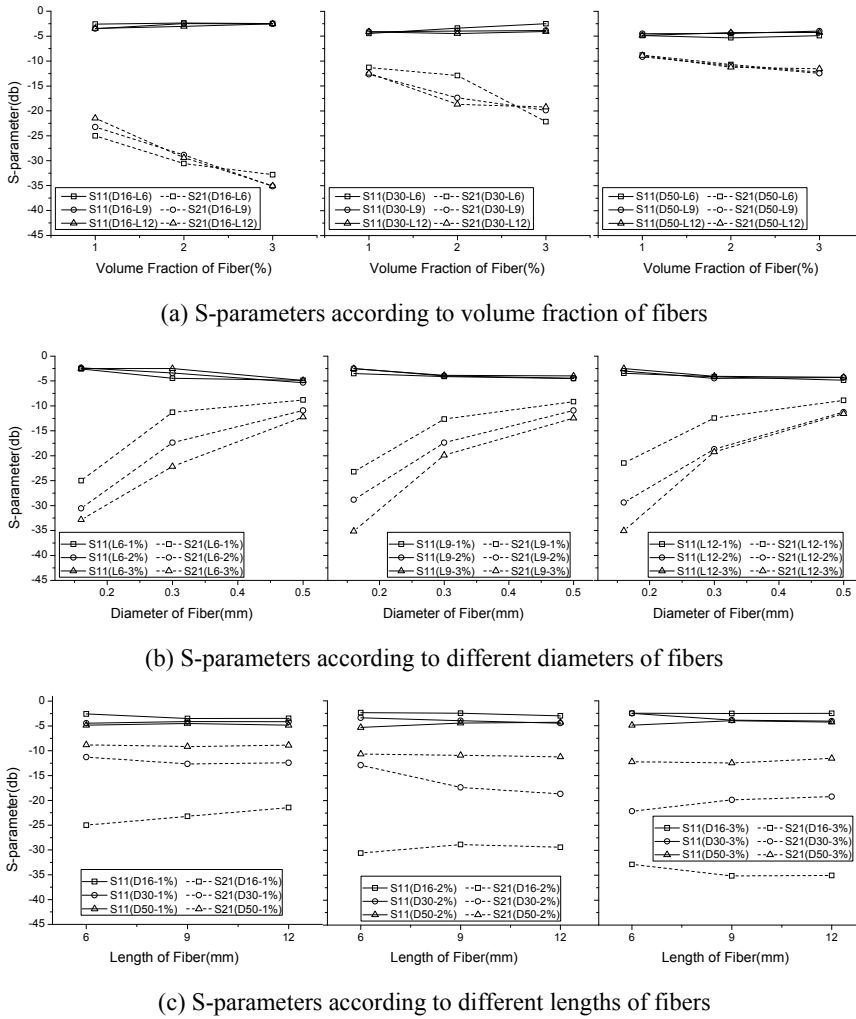


Figure 9: S-parameters averaged over a frequency range from 8.1 to 12.5GHz

5.3 Shielding effectiveness according to the number of fibers

The variations of the S-parameter and permittivity according to the analysis of parameters are portrayed in Figs. 8 to 12. Another important factor is the number of fibers in a specimen, listed in Tab. 2. The S-parameters and permittivity are plotted over the number of fibers in Figs. 13 and 14, respectively.

Figure 13 reveals a definite influence of the number of fibers on the S-parameters. The rate of change of the S11 and S21 parameters, respectively, is shown to be very steep until a concentration of around 400 fibers; thereafter, the S11 and S21 parameters change only gradually with an increase of the number of fibers. This means that shielding effectiveness is not significantly enhanced beyond a certain number of fibers. The results in Fig. 13 could be used as fundamental data in determining the optimal amount of fibers to shield electromagnetic waves while obtaining required mechanical performance.

A noteworthy feature of the real part of the relative permittivity is found in Fig. 14(a). The real part increased at the beginning with an increase of the number of fibers, but remained at a lower and constant value beyond 400 fibers. Meanwhile, the increase rate of the imaginary part is very steep under about 400 fibers and is reduced thereafter, which corresponds to the trend for specimens D16-L9-2% and D16-L12-2%. This variation of the imaginary part might be explained by the increase of conductivity. The imaginary part of permittivity is related to the loss or dissipation of electric energy. The conductivity of the mortar is increased with the increase of fiber content, and the dissipated energy is also increased. The abrupt drop of the real part indicates that there is a threshold for the number of fibers in enhancing the shielding effectiveness, and this drop might be due to the fact that the internal scattering of the wave entrapped by the steel fibers in the mortar increased when exceeding a certain number of fibers.

Based on the results in Fig. 14, it can be concluded that within the scope of this study the optimal number of fibers for shielding is around 400, at which S21 is about -30dB, indicating that the electric field intensity of the incident wave is reduced as much as 97%.

6 Conclusions and future study

The effects of diameter, length, and volume fraction of steel fibers on electromagnetic shielding effectiveness in steel fiber-reinforced mortar were numerically investigated in this study. Some of the analysis results were compared with test results to verify the analysis method. The comparison showed good agreement between the calculated and the measured results. From the analysis results, the following salient features were found.

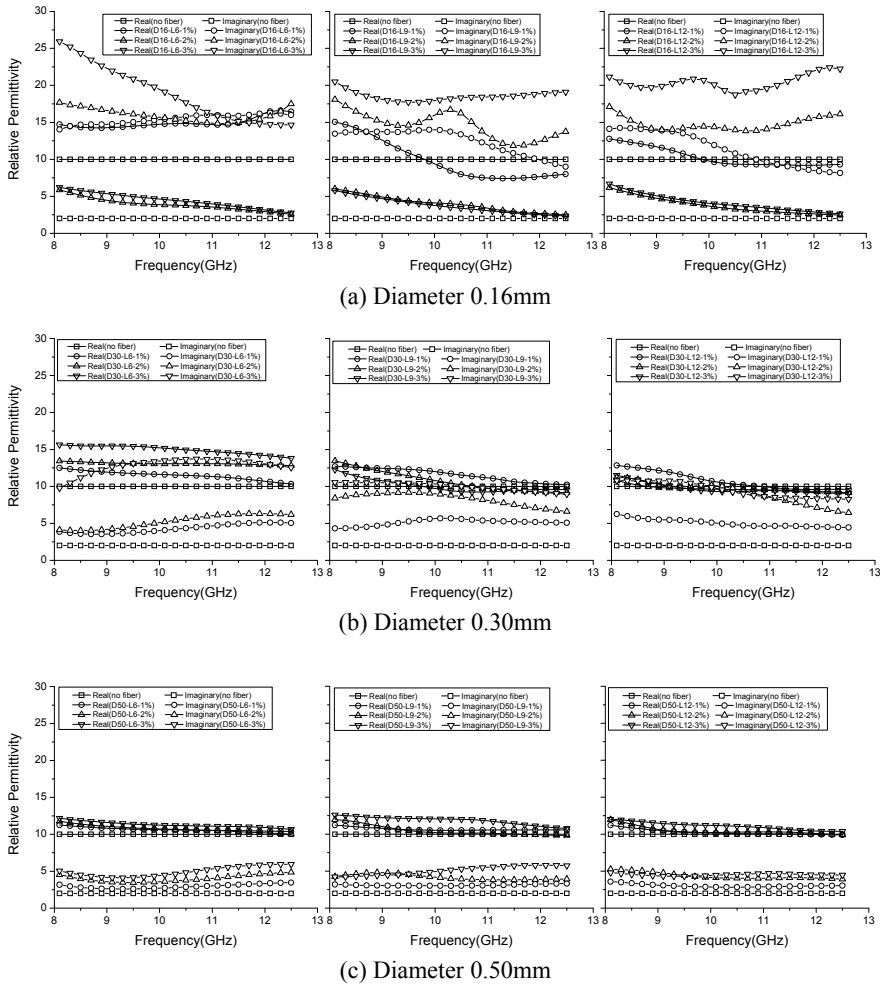
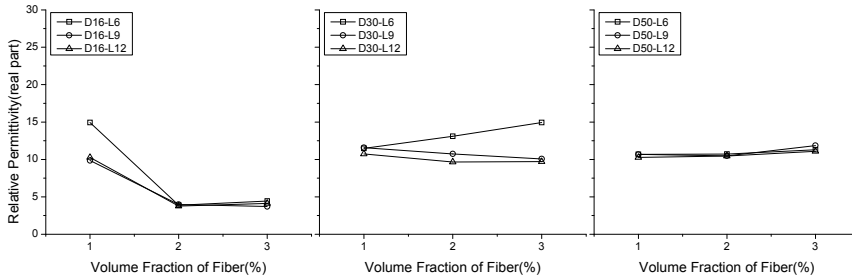
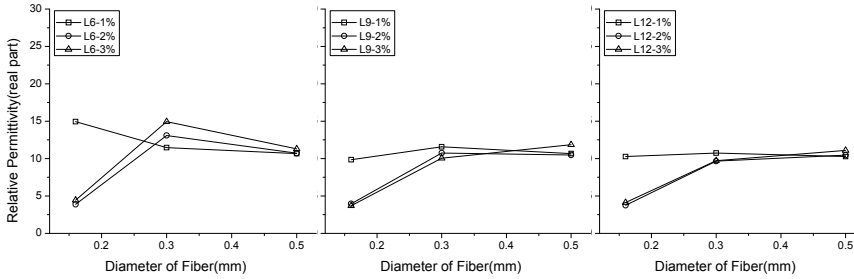


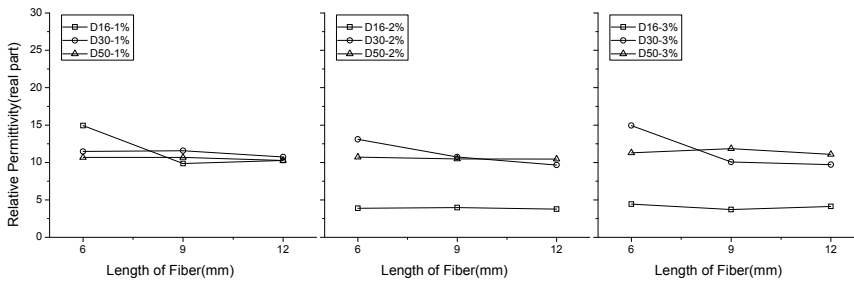
Figure 10: Permittivity determined from S-parameters



(a) Real part of relative permittivity according to different volume fractions of fibers

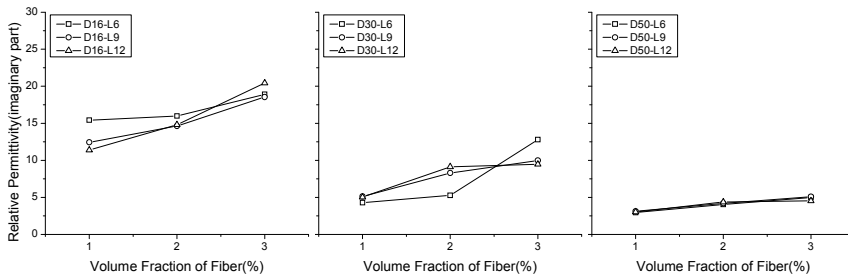


(b) Real part of relative permittivity according to different diameters of fibers

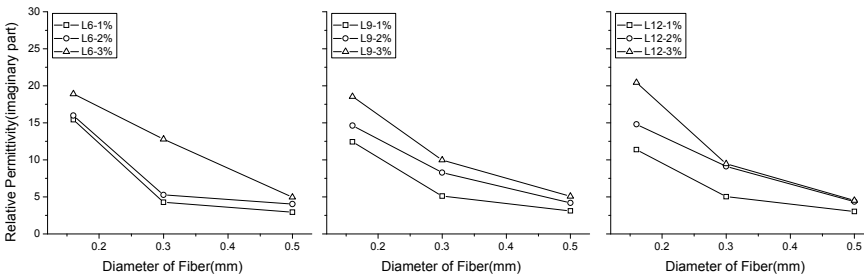


(c) Real part of relative permittivity according to different lengths of fibers

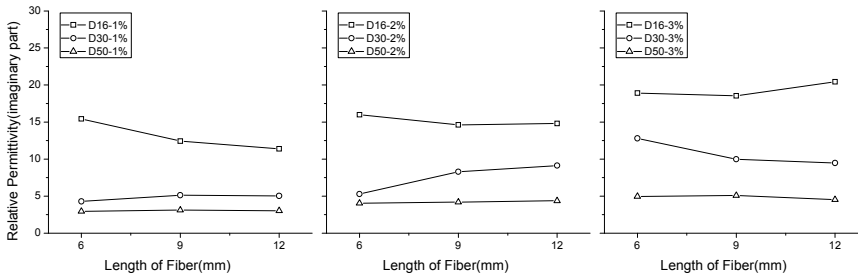
Figure 11: Real part of relative permittivity



(a) Imaginary part of relative permittivity according to different volume fractions of fibers



(b) Imaginary part of relative permittivity according to different diameters of fibers



(c) Imaginary part of relative permittivity according to different lengths of fibers

Figure 12: Imaginary part of relative permittivity

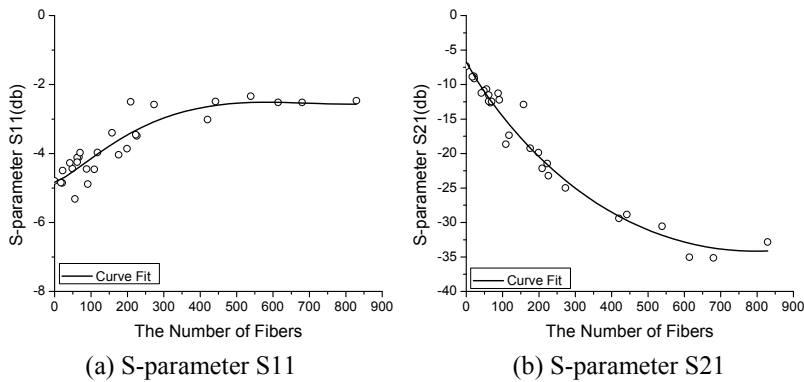


Figure 13: Variation of S-parameters according to the number of fibers

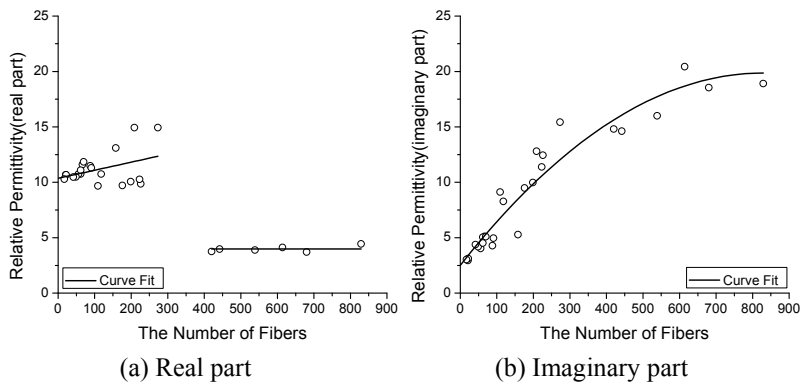


Figure 14: Variation of relative permittivity according to the number of fibers

1. The number of fibers is a very important factor influencing the degree to which electromagnetic waves are shielded, and the optimal number of fibers inserted in a specimen with dimensions of $19 \times 18 \times 5$ mm is about 400, at which S21 is about -30dB, that is, 97% reduction in electric field intensity.
2. The real part of permittivity increased at the beginning with an increase of the number of fibers, but remained at a lower and constant value beyond 400 fibers. Meanwhile, the increase rate of the imaginary part is steep under about 400 fibers and is reduced thereafter.

3. The rate of change of the S11 and S21 parameters, respectively, is very steep until a concentration of around 400 fibers; thereafter, the S11 and S21 parameters change only gradually with an increase of the number of fibers.
4. Smaller fiber diameters and larger fiber volume fractions provide better shielding effectiveness.
5. Fiber length does not strongly influence shield effectiveness.
6. At a diameter of 0.16mm, 2% volume fraction, and length exceeding 9mm, 97% shielding effectiveness for the electric field intensity can be achieved.

In order to extensively investigate the shielding effectiveness of cement-based materials reinforced with steel fibers and to examine an applicability of those materials in practice, computational and experimental works considering more parameters than those considered in this study will be planned in the near future.

Acknowledgement: This work was supported by the IT R&D program of MKE/IITA [2008-F-044-01, Development of new IT convergence technology for smart building to improve the environment of electromagnetic waves, sound and building] and by the Korea Science and Engineering Foundation (KOSEF) grant funded by the Korea government (MEST20090080587). The authors would like to thank Dr. Il Sung Seo in Agency for Defense Development (ADD) and Mr. Bong-Rae Kim at KAIST for conducting the experiment.

References

- Bazant, Z.P.; Planas, J.** (1998): Fracture and Size Effect in Concrete and Other Quasibrittle Materials. CRC Press.
- Baker-Jarvis, J.; Vanzura, E.J.; Kissick, W.A.** (1990): Improved technique for determining complex permittivity with the transmission/reflection method. *IEEE Transactions on Microwave Theory and Technique*, vol. 38, pp. 1096–1103.
- Brown, K.M.** (1970): Derivative-free analogues of the levenberg, Marquardt and Gauss Algorithms for Non-linear Least Square Approximations. *IBM, Philadelphia Scientific Center Technical Report*, No. 320–2994.
- Bois, K.J.; Benally, A.D.; Nowak, P.S.; Zoughi, R.** (1998): Cure-state monitoring and water-to-cement ratio determination of fresh Portland cement-based materials using near-field microwave techniques. *IEEE transactions on Instrumentation and Measurement*, vol. 47, pp. 628–637.
- Charkrabarty, A.; Cargin, T.** (2008): Computational studies on mechanical and

thermal properties of carbon nanotube based nanostructures. *CMC: Computers, Materials, & Continua*, vol. 7, pp. 167–190.

Chiou, J.-M.; Zheng, Q.; Chung, D.D.L. (1989): Electromagnetic interference shielding by carbon fiber-reinforced cement. *Composites*, vol. 20, pp. 379–381.

Fu, X.; Chung, D.D.L. (1997): Submicron carbon filament cement-matrix composites for electromagnetic interference shielding. *Cement and Concrete Research*, vol. 26, pp. 1467–1472.

Fu, X.; Chung, D.D.L. (1989): Submicron-diameter-carbon-filament cement-matrix composites. *Carbon*, vol. 36, pp. 459–462.

Felekoglu, B.; Turkel, S.; Altuntas, Y. (2007): Effects of steel fibers reinforcement on surface wear resistance of self-compacting repair mortars. *Cement and Concrete Composites*, vol. 29, pp. 391–396.

Ferretti, E.; Leo, A.D. (2008): Cracking and creep role in displacements at constant load: concrete solids in compression. *CMC: Computers, Materials, & Continua*, vol. 7, pp. 59–80.

Ghanbari, J.; Naghdabadi, R. (2009): Multiscale nonlinear constitutive modeling of carbon nanostructures based on interatomic potentials. *CMC: Computers, Materials, & Continua*, vol. 10, pp. 41–64.

Gonzalez, E.V.; Maimi, P.; Turon, A.; Camanho, P.P.; Renart, J. (2009): Simulation of delamination by means of cohesive elements using an explicit finite element code. *CMC: Computers, Materials, & Continua*, vol. 9, pp. 51–92.

Ghodgaonkar, D.K.; Varadan, V.V.; Varadan, V.K. (1989): A free-space method for measurement of dielectric constants and loss tangents at microwave frequencies. *IEEE Transactions on Instrumentation and Measurement*, vol. 37, pp. 789–793.

HFSS. (2008): High Frequency Structure Simulation. *Ansoft Inc.*

Halabe, U.B.; Sotoodehnia, A.; Maser, K.R.; Kausel, E.A. (1993): Modeling the electromagnetic properties of concrete. *ACI Materials Journal*, vol. 90, pp. 552–563.

Kim, P.C.; Lee, D.G. (2009): Composite sandwich constructions for absorbing the electromagnetic waves. *Composite Structures*, vol. 87, pp. 161–167.

Li, S.X.; Zhao, L.; Liu, Y.W. (2008): Computer simulation of random sphere packing in an arbitrary shaped container. *CMC: Computers, Materials, & Continua*, vol.7, pp. 109–118.

Mai-Duy, N.; Khennane, A.; Tran-Cong, T. (2007): Computation of laminated composite plates using integrated radial basis function networks. *CMC: Computers, Materials, & Continua*, vol. 5, pp. 63–78.

Oh, J.; Katsube, N.; Brust, F.W. (2007): Numerical analysis of the effect of diffusion and creep flow on cavity growth. *CMC: Computers, Materials, & Continua*, vol. 6, pp. 129–158.

Pozar, David M. (2005): *Microwave Engineering-3rd ed.* John Wiley & Sons, Inc.

Rahimi, M.M.; Kesler, C.E. (1979): Partially steel-fibers reinforced mortar. *ASCE Journal of the Structural Division*, vol. 105, pp. 101–109.

Shah, S.P.; Naaman, A.E. (1976): Mechanical properties of glass and steel fibers reinforced mortar. *ACI Journal Proceedings*, vol. 73, pp. 50–53.

Seo, I.S.; Chin, W.S.; Lee, D.G. (2004): Characterization of electromagnetic properties of polymeric composite materials with free space method. *Composite Structures*, vol. 66, pp. 533–542.

Timmel, M.; Kaliske, M.; Kolling, S.; Mueller, R. (2007): A micromechanical approach to simulate rubberlike materials with damage. *CMC: Computers, Materials, & Continua*, vol. 5, pp. 161–172.

Wen, S.; Chung, D.D.L. (2004): Electromagnetic interference shielding reaching 70 dB

in steel fibers cement. *Cement and Concrete Research*, vol. 34, pp. 329–332.

Wittmann, F.H. (1975): Microwave Absorption of Hardened Cement Paste. *Cement and Concrete Research*, vol. 1, pp. 63–71.

Xie, C.Q.; Han, X.; Long, S.Y. (2007): Characteristic of waves in a multi-walled carbon nanotube. *CMC: Computers, Materials, & Continua*, vol. 10, pp. 1–12.

